

# Facile Preparation of Drug-Loaded Tristearin Encapsulated Superparamagnetic Iron Oxide Nanoparticles Using Coaxial Electro spray Processing

Manoochehr Rasekh,<sup>\*,†</sup> Zeeshan Ahmad,<sup>\*,‡</sup> Richard Cross,<sup>§</sup> Javier Hernández-Gil,<sup>†</sup> James D. E. T. Wilton-Ely,<sup>\*,†</sup> and Philip W. Miller<sup>\*,†</sup>

<sup>†</sup>Department of Chemistry, Imperial College London, South Kensington, London SW7 2AZ, U.K.

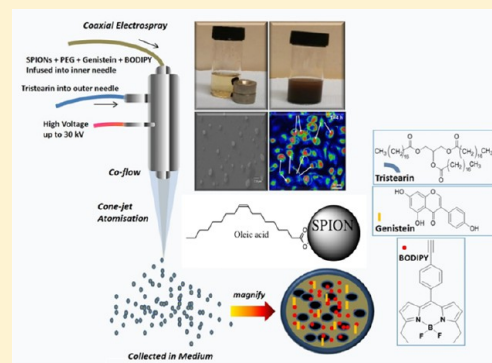
<sup>‡</sup>Leicester School of Pharmacy, De Montfort University, Leicester LE1 9BH, U.K.

<sup>§</sup>Emerging Technologies Research Centre, De Montfort University, Leicester LE1 9BH, U.K.

## Supporting Information

**ABSTRACT:** Naturally occurring polymers are promising biocompatible materials that have many applications for emerging therapies, drug delivery systems, and diagnostic agents. The handling and processing of such materials still constitutes a major challenge, which can limit the full exploitation of their properties. This study explores an ambient environment processing technique: coaxial electro spray (CO-ES) to encapsulate genistein (an isoflavonoid and model drug), superparamagnetic iron oxide nanoparticles (SPIONs, 10–15 nm), and a fluorophore (BODIPY) into a layered (triglyceride tristearin shell) particulate system, with a view to constructing a theranostic agent. Mode mapping of CO-ES led to an optimized atomization engineering window for stable jetting, leading to encapsulation of SPIONs within particles of diameter 0.65–1.2  $\mu\text{m}$  and drug encapsulation efficiencies of around 92%. Electron microscopy was used to image the encapsulated SPIONs and confirm core–shell triglyceride encapsulation in addition to further physicochemical characterization (AFM, FTIR, DSC, and TGA). Cell viability assays (MTT, HeLa cells) were used to determine optimal SPION loaded particles ( $\sim 1$  mg/mL), while *in vitro* release profile experiments (PBS, pH = 7.4) demonstrate a triphasic release profile. Further cell studies confirmed cell uptake and internalization at selected time points ( $t = 1, 2,$  and  $4$  h). The results suggest potential for using the CO-ES technique as an efficient way to encapsulate SPIONs together with sensitive drugs for the development of multimodal particles that have potential application for combined imaging and therapy.

**KEYWORDS:** encapsulation, electro spraying, imaging, drug delivery, nanoparticle, theranostics



## INTRODUCTION

Advances in nanotechnology continue to have a tremendous impact on medicine. In particular, new approaches for targeted drug delivery and biomedical imaging sciences have benefited from the development of inorganic and organic based nanoparticles (NPs).<sup>1–5</sup> NPs for medical use are typically composed of an inorganic or organic matrix material that is functionalized with a drug and/or a targeting agent. Superparamagnetic iron oxide nanoparticles (SPIONs) have been widely investigated as contrast agents for magnetic resonance imaging (MRI) due to their ability to significantly reduce spin–spin relaxation ( $T_2$ ) times required for magnetic resonance (MR) contrast enhancement.<sup>6–8</sup> External magnetic fields can also be used to guide these nanoparticles to targets within the body and then used to induce local hyperthermia to destroy cells. Their low toxicity coupled with their ease of synthesis also makes them highly attractive for such therapeutic and diagnostic applications. The nanostructure of SPIONs is typically based on an inorganic maghemite ( $\gamma\text{-Fe}_2\text{O}_3$ ) and/or

magnetite ( $\text{Fe}_3\text{O}_4$ ) core and can vary in size from 2 nm to microns depending on the synthesis method. The high surface-to-volume ratio of SPIONs typically result in aggregation; hence, coating with a suitable biocompatible material is necessary to ensure discrete particle formation. Hydrophilic polymers such as polyethylene-glycol (PEG), PEG/polyethylene-imine copolymers, dextran, or chitosan are often used to inhibit aggregation and to ensure water solubility. Functionalizing the shell of NPs is also an important strategy for improving targeting ability, drug encapsulation, and controlled release. There are a number of techniques to combine targeting molecules and drugs with nanoparticles; these include various bioconjugation methods, electrostatic interactions, co-loading of drugs into the polymer shell matrix and adsorption into hollow

**Received:** February 12, 2017

**Revised:** April 18, 2017

**Accepted:** April 26, 2017

**Published:** April 26, 2017

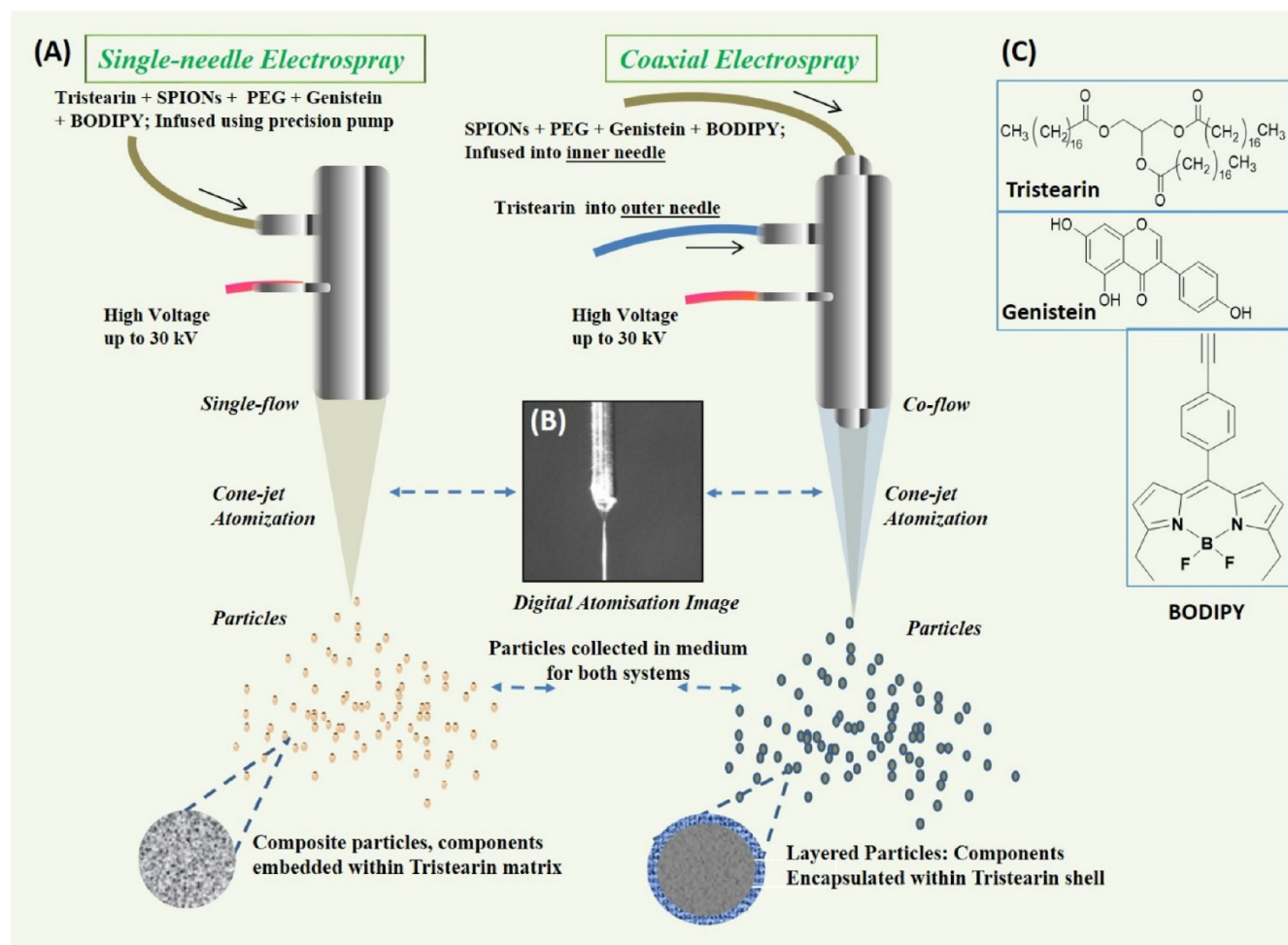


**Figure 1.** Schematic of electro spray setup. (A) Single needle and coaxial electro spraying devices. (B) Close-up image of the atomization process (stable cone-jet mode). (C) Key materials used.

or mesoporous structures.<sup>9</sup> Several recent examples of drug loaded SPIONs have shown excellent targeting efficiencies and anticancer effects with minimal systemic toxicity.<sup>10–14</sup>

The protection afforded by the coating to the NP carrier matrix can lead to the more selective delivery of active components, enhance drug efficacy, and reduce toxicity.<sup>15</sup> Tristearin is a lipid commonly used to prepare solid–lipid nanoparticles (SLNs) for the development of drug delivery carriers. SLNs are biocompatible, biodegradable, and physicochemically stable with a low toxicity. They are promising drug carrier systems, particularly for applications that require sustained release.<sup>16–18</sup> Recently, the encapsulation of aloemodin (AE) in SLNs, using a high-pressure homogenization technique, has been demonstrated to improve its anticancer efficacy.<sup>19</sup> AE has poor water solubility, low absorption, and bioavailability issues that have limited its clinical applications. AE-SLNs showed much higher *in vitro* cytotoxicity against several human cancer lines compared to AE solutions alone, with the improved efficacy being attributed to the increased cellular uptake of AE as a result of the SLN formulation.

Consistent and reproducible control over drug loading and particle size are still challenging; hence, new methods that are better able to provide this control and can be generally applied to a range of particle types and drug molecules are highly sought after. Electrohydrodynamic atomization (EHDA) (or electro spray) involves the application of an electric field to a

flowing electrically conductive liquid (or coflow system) in order to generate micro- or nanosized particles; it is finding increasing applications in emerging pharmaceutical technologies.<sup>20</sup> This technique has been demonstrated by some of us in a variety of novel biomedical applications.<sup>21–23</sup> Herein, we report the use of a coaxial electro spray (CO-ES) technique to generate multimodal submicron-to-micron sized particles combining a SPION core with an optical probe integrated into a tristearin shell. A model drug compound (genistein) was also encapsulated into a core–shell material using this electro spray technique and the drug release profile, and cellular uptake of the particles was investigated.

## ■ MATERIALS AND METHODS

**Chemicals and Reagents.** Tristearin ( $\geq 99\%$ ,  $M_w$  891.48 g/mol) and PEG ( $M_w$  20000 g/mol) were purchased from Sigma-Aldrich, Dorset, U.K. Genistein ( $\geq 98\%$  purity,  $M_w$  = 270.24 g/mol, crystal powder form) was purchased from VWR International Ltd., Leighton Buzzard, U.K. SPIONs<sup>24</sup> and ethynyl-boron-dipyrromethene (BODIPY) fluorescent dye<sup>25</sup> were synthesized using methods based on literature protocols. 1-(4,5-Dimethylthiazol-2-yl)-3,5-diphenylformazan (MTT, Thiazolyl blue formazan),  $\text{FeCl}_2$  (98%),  $\text{FeCl}_3$  (97%),  $\text{NH}_4\text{OH}$  (ammonium hydroxide solution/ACS reagent, 28.0–30.0%  $\text{NH}_3$  basis) and oleic acid ( $\geq 99\%$ ) were all purchased from Sigma-Aldrich, Dorset, U.K. Solvents were obtained from

commercial sources and used as received without additional purification.

**Synthesis of Superparamagnetic Iron Oxide Nanoparticles (SPIONs).** Iron(II) chloride (0.63 g, 5.0 mmol) was dissolved in HCl (2.5 mL, 5.0 mmol) to give a 2 M yellow solution. Iron(III) chloride (1.62 g, 10.0 mmol) was dissolved in deoxygenated water (10 mL) to give a 1 M orange solution. The solutions were mixed together and added to a 0.7 M ammonium hydroxide solution (125 mL, 87.5 mmol). The mixture was then stirred vigorously for 30 min. The resulting black precipitate was separated magnetically (0.80 g, 70%). The capping agent, oleic acid (1.6 mL, 5.0 mmol), was dissolved in acetone (5 mL) and added dropwise to the separated black precipitate, and the mixture was then heated at 80 °C for 30 min and the resulting precipitate separated magnetically again and washed with acetone and then dissolved in 50 mL of toluene. The resulting solution was centrifuged at 4000 rpm for 1 h to separate any precipitates, and the supernatant liquid was collected and then evaporated to dryness to give the SPIONs<sup>26</sup> (Supporting Information, Figure S1).

**Preparation of Electrospray Solutions.** A series of solutions was prepared for the electrospray (ES) process. Tristearin was dissolved in dichloromethane (2 w/v %) through mechanical stirring at ambient temperature (22 °C). PEG was added to ethanol (5 w/v %) and stirred vigorously for 30 min. Genistein was then dissolved (1 mg/mL) in the PEG solution with mechanical stirring for 30 min. The synthesized SPIONs were suspended in the final solution and sonicated for 5 min.

**Characterization of Electrospray Solutions.** The electrospray solutions were characterized for density, surface tension, viscosity, and electrical conductivity. Density values were obtained using standard 25 mL pycnometers (VWR, Leicestershire, U.K.). The surface tension of the solutions was measured using a 0/80256E Balance Tensiometer (White Elec. Inst. Co., Ltd., Worcestershire, U.K.) using the Du Noüy platinum ring technique. The solution viscosities were measured using a SV-10 Sine-wave Vibro-Viscometer (A&D, Oxfordshire, U.K.). A FG3-FIVEGO conductivity meter (Mettler Toledo, Leicester, U.K.) was used to measure the electrical conductivity of the solutions. The mean value of five consecutive readings was used in all cases.

**Encapsulation of SPIONs.** The coaxial electro-spraying device consists of two concentrically aligned stainless steel capillary needles with outer diameters of 0.9 and 1.9 mm, respectively. The needle was connected to a high voltage supply (up to 30 kV, 1.5 mA, Glassman High Voltage Supply, U.K.). The solutions were perfused using a syringe pump (World Precision Instruments, Florida, US). The deposition distance for the encapsulation of SPIONs and genistein was kept at 100 mm from the tip of the needle to the collection substrate, and the samples were collected in a glass vial (15 mL of deionized water). The experiments were carried out at ambient temperature (22 °C). The single needle and coaxial electro-spraying setup are shown in Figure 1.

**Jetting and Mode Mapping.** Jetting and mode mapping were studied to optimize the EHDA process. For this, four individual processing materials were studied, which included the optimized formulation, a suspension containing SPIONs, and a PEG/ethanol solution. The mode mapping procedure involves assessment of the jetting mode at incremental changes to flow rate and applied voltage. It was anticipated that there would be an impact on jet formation as a result of changes in electrical conductivity and surface tension due the presence of

SPIONs. To ensure optimum jetting behavior, a camera (Samsung NX 2000, 21.6 MP/APS-C sensor, Korea) was used to capture digital images of jetting modes.

**Spectral and Thermal Characterization.** Differential scanning calorimetry (DSC) analysis of the samples (raw materials and encapsulated particles) was carried out using a Jade DSC PerkinElmer 204 F1 Phoenix (Netzsch, Selb, Germany) instrument at a heating rate of 10 °C/min under a nitrogen purge of 70 mL/min from 20 to 300 °C. The physical properties of the samples were also characterized by thermogravimetric analysis (TGA) using a PerkinElmer-Thermogravimetric analyzer (Pyris, Germany). Fourier transform infrared (FTIR) spectra of raw materials and encapsulated SPIONs were recorded using a PerkinElmer (Analytical Siemens, USA) with a resolution of 2 cm<sup>-1</sup>. The spectra were recorded between 4000 and 650 cm<sup>-1</sup> after correction of the baseline.

**Electron Microscopy Analysis and Zeta Potential Measurement.** Scanning electron microscopy (SEM) was carried out using a Zeiss-EVO LS 15 instrument (Germany), operated at an accelerating voltage of 10 kV to study the size and surface morphology of the particles. Samples were gold coated using a rotary-pumped sputter coater (Q150R ES, Quorum Technologies Ltd., East Sussex, U.K.) to improve the conductivity of the surface of the sample and to prevent overcharging. Transmission electron microscopy (TEM) was performed using a JEOL TEM 2100F (JEOL Ltd., Japan) instrument with an operating voltage of 200 kV. Atomic force microscopy (AFM) measurements were performed using a Park AFM XE-100 series scanning probe microscope. All images were taken in true noncontact mode with a scan rate of 0.5 Hz at room temperature and pressure using a commercial silicon cantilever (Innovative Solutions, Bulgaria). No modifications were made to the samples prior to imaging. All processing and analysis of the data was undertaken using the Park AFM XEI software. The particle size and size distribution of the particles were measured by Carl Zeiss SmartTiffV3 software. These measurements were performed in triplicate. Zeta potential ( $\zeta$ -potential) studies for core-shell encapsulated nanoparticles and blank tristearin particles were performed using a Nanobrook Omni analyzer (Nanobrook Omni, Brookhaven, US). The mean  $\pm$  standard deviation of ten replicates was obtained. Particles were analyzed in phosphate buffered saline (PBS, pH = 7.4).

**Drug Encapsulation and Release Study.** The genistein loading in the tristearin particles was calculated based on eq 1.

$$\begin{aligned} \text{encapsulation efficiency (\%)} &= \frac{\text{total concentration of drug} - \text{concentration of free drug}}{\text{total concentration of drug}} \\ &\times 100 \end{aligned} \quad (1)$$

Two types of genistein formulation were evaluated for release kinetics. These were a composite tristearin/SPIONs (single-needle electrospray) combination and a final encapsulation formulation (coaxial electrospray/CO-ES). In the latter case, a known quantity of genistein-loaded particles was dissolved in ethanol under mechanical stirring for 2 h and a UV-vis spectrophotometer ( $\lambda = 260$  nm) was used to determine the concentration of the drug in the final formulation. The theoretical value was calculated based on the infusion of a known concentration of the final formulation of material.

Table 1. Physical Properties of the Solutions and Solvents

solvent or solution	density (kg m <sup>-3</sup> )	surface tension (mN m <sup>-1</sup> )	viscosity (mPa s)	electrical conductivity 10 <sup>-2</sup> (Sm <sup>-1</sup> )
tristearin/DCM (2 w/v %)	1293 ± 0.44	35.10 ± 0.66	2.91 ± 0.01	0.002 ± 0.0002
PEG/ethanol (5 w/v %)	996 ± 0.55	66.59 ± 0.38	3.82 ± 0.02	0.003 ± 0.0011
[PEG/ethanol] + SPIONs (0.5 w/v %)	1001 ± 0.66	62.88 ± 0.19	3.81 ± 0.02	0.010 ± 0.0002
dichloromethane (DCM)	1321 ± 1.7	40.76 ± 0.45	2.14 ± 0.02	0.001 ± 0.0002
ethanol	790 ± 1.17	25.41 ± 0.16	1.30 ± 0.01	0.091 ± 0.0010

For release studies, 1 mL of formulation was electrospayed directly into 10 mL of PBS (pH = 7.4) using the CO-ES technique. The same process was carried out for the composite tristearin/SPIONs composition using single-needle electro-spray. The concentration of genistein in the formulation was 1 mg/mL. Once the electrospaying (ES) process was completed, the particle-released medium mixture was placed into a shaking water bath at 37 °C (Stuart SB 540, U.K.). At defined time intervals, the PBS–particle mixture was removed and centrifuged (Eppendorf, centrifuge 5702, Germany) at 1000 rpm for 5 min. A pipet was used to remove 1 mL for UV measurement. Fresh PBS medium (1 mL) was added to the existing PBS–particle solutions before returning them to the water bath. The release of genistein was carried out over a 30 h period in triplicate. For active release *in vitro* studies the number of replicates was 3 ( $n = 3$ ).

**Cell Culture.** To assess the potential biocompatibility of the encapsulated SPIONs, the HeLa cell line was used.<sup>27</sup> HeLa cells were cultured in Dulbecco's Modified Eagle's Medium, supplemented with 10% fetal calf serum, 1% nonessential amino acids, L-ascorbic acid (0.150 g/L), 2 mM L-glutamine, 0.02 M HEPES, penicillin (100 units/mL), and streptomycin (0.1 mg/mL) (all purchased from Sigma, Dorset, U.K.). HeLa cells were maintained at 37 °C in a humidified incubator with 5% CO<sub>2</sub>.

**MTT Cytotoxicity Assay.** HeLa cells were seeded at  $1 \times 10^5$  cells per well using a 96-well plate (Nunc, Fisher Scientific, Loughborough, U.K.) and were incubated for 24 h in culture media. One hundred microliters of the encapsulated SPIONs (CO-ES) and electrospayed tristearin NPs (single-needle electro-spray) were added to selected wells at concentrations of 0.1, 0.25, 0.5, and 1 mg/mL. The cells were further incubated for 24 h, and then 50  $\mu$ L of MTT reagent (prepared in a physiological solution) were then added to cells and incubated for 2 h according to the manufacturer's instructions. The negative control contained media only. After 2 h of MTT incubation, the culture media were removed, and cells were washed with 100  $\mu$ L of PBS prior to the addition of 100  $\mu$ L of dimethyl sulfoxide (DMSO) to each well to dissolve formazan precipitates. The quantity of formazan, which is proportional to the number of viable cells, was measured via the change in absorbance at 570 nm using a SpectraMax M2e Multimode Microplate Reader with SoftMax Pro Software (Molecular Devices, VWR, West Sussex, U.K.).

**T<sub>2</sub> Relaxivity Measurements.** Relaxivity measurements at a magnetic field of 9.4 T (400 MHz) were performed in an NMR spectrometer (Bruker AV400, Germany) at room temperature with a standard Carr Purcell Meiboom Gill (CPMG) sequence. The relaxivity constant ( $r_2$ ) was calculated from the slope of the curve obtained by fitting the  $(T_2)^{-1}$  values versus the total Fe concentration in millimolar of encapsulated SPIONs (0, 0.54, 1.1, 2.15, 4.31 mM).

**Confocal Imaging and Cellular Uptake.** Confocal microscopy was performed on a CF4-Leica SPS inverted

confocal microscope (Leica, Germany) with a tunable infrared laser for multiphoton imaging, motorized stage, and full incubation chamber. Cell suspensions were prepared at a concentration of  $1 \times 10^4$  cells per well and seeded to 6-well plates (Nunc, Fisher Scientific, Loughborough, U.K.), each containing an autoclaved 13 mm coverslip. After 24 h of incubation, 100  $\mu$ L of encapsulated SPIONs (1 mg/mL) were added to each of the wells at different time points (1, 2, and 4 h) and incubated for another 24 h. After 24 h, the media were removed, and the cells were washed with PBS twice and then fixed using Alfa Aesar Paraformaldehyde, 4% in PBS–paraformaldehyde (Fisher Scientific, Loughborough, U.K.). A drop of AF1 Citifluor antifadent mountant (Agar Scientific Ltd., Essex, U.K.) was added to a microscope slide and the coverslip placed on it (cell side down) prior to microscopy.

**Statistical Analysis.** The data from the MTT cytotoxicity assay were analyzed statistically using one-way ANOVA with Bonferroni post hoc test;  $p < 0.05$  was considered as statistically significant. The criterion for statistical difference between groups was  $p < 0.05$ . The statistical tests were performed using Prism 7.01 (GraphPad, San Diego, CA, USA).

## RESULTS AND DISCUSSION

**Synthesis of SPIONs.** Superparamagnetic iron oxide nanoparticles (SPIONs) were synthesized using the method described by Feng et al.<sup>26</sup> The SPIONs possessed a mean size range of 10–15 nm as determined by TEM. UV–vis spectroscopy further confirmed the synthesis of SPIONs<sup>28</sup> (Supporting Information, Figure S2).

**Excipient Suitability.** Formulation of excipient media used for particle engineering has been explored for numerous *in vitro* and *in vivo* studies. For example, genistein has been explored for chemotherapeutic applications and is known to be an excellent molecule for several other biological functions.<sup>29</sup> Similarly, tristearin has been explored in numerous therapeutic dosage forms involving solid lipid nanoparticles<sup>30</sup> and as solid oral drug delivery systems (e.g., tablets)<sup>31</sup> displaying good *in vitro* and *in vivo* outcomes. SPIONs have been investigated as nontoxic MRI imaging agents and theranostic agents. PEG is a widely used excipient in pharmaceutical formulations, while BODIPY has excellent optical properties for cellular imaging.

**Materials Characterization.** The physical properties of the materials are important indicators for ES processing suitability. The ES processing of solutions relies on the relationship of surface tension, density, and electrical conductivity to determine jet formation and stability. During jet formation, the electrical force applied results in deformation of the liquid into a cone if the solution is sufficiently electrically conducting. Surface tension counteracts the action of the electric field enabling the formation of a stable cone jet. The applied electrical force must exceed the surface tension in order to generate a spray. Therefore, materials possessing a surface tension less than water (70 mN/m) are ideal for ES. All solutions in this study demonstrated electrical conductivity

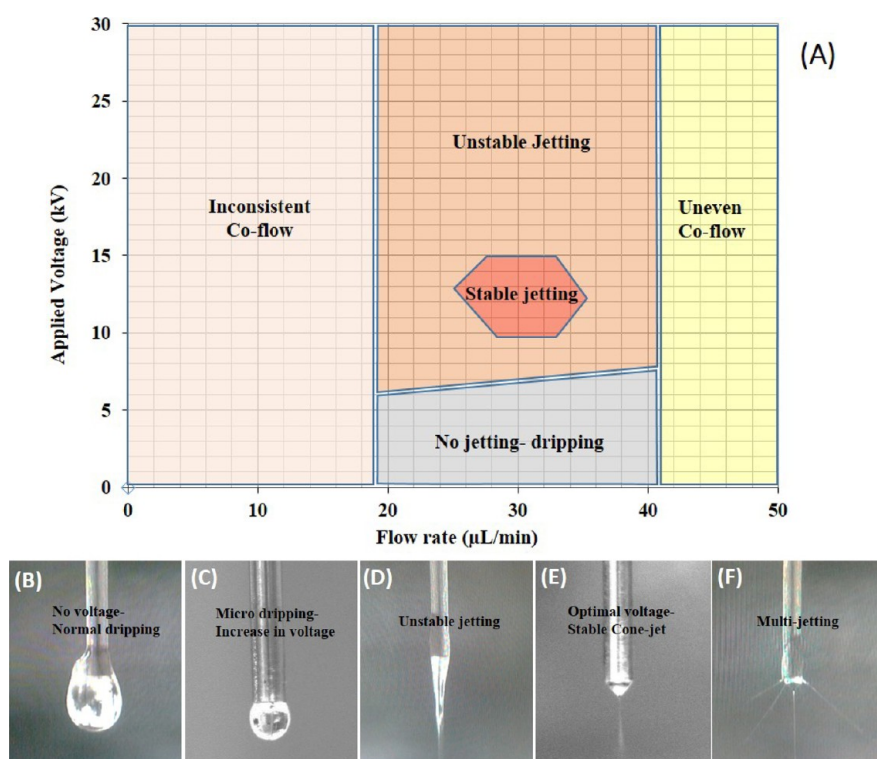


**Figure 2.** Mode mapping (A) and jetting modes (B–F) of the electrospaying (ES) process.

values in suitable ranges for ES. Ethanol-based formulations have been used extensively in ES investigations,<sup>32</sup> though dichloromethane, which has a lower electrical conductivity than ethanol, has also been employed for matrix-type nanoparticle formulations.<sup>33</sup> The surface tension of all suspension and processing media used in this work were below 70 mN/m in order to ensure their suitability for the ES process. All solutions demonstrated low viscosity when compared to previous studies used for electrospinning fibers.<sup>22</sup> Viscosity is an important parameter as it is often used to determine the morphology of ES media. Most polymeric solutions with a high molecular weight will yield fibers. In this study, the low viscosities will ensure particle synthesis will result in preference to fiber formation. Table 1 details the main physical properties of solutions and solvents used in this study.

**Jetting and Mode Mapping (Spraying Stability).** Based on the values (applied voltage vs flow rate), all formulations were subjected to mode mapping and ES optimization. For the PEG/ethanol formulation, the flow rate (1–45 μL/min) and applied voltage (0–30 kV) were selected. A camera was used to provide continuous monitoring of the jetting behavior over time. The jetting behavior of the PEG/ethanol solution is shown in the Supporting Information (Figure S3A and Table S1A) and follows a clear trend. When the flow rate is below 6.5 μL/min, inconsistent results are observed, suggesting that the infusion is insufficient to force the medium out of the nozzle continuously. This affects the particle size, as the true flow rate is not observed. Consistent flow from the needle was observed with flow rates in the range 10–45 μL/min, while values beyond this flow rate produced jetting instability. Between the applied voltages 12–24.1 kV and a flow rate of 10 to 45 μL/min, a stable jetting window was established. On either side of this applied voltage range (e.g., <12 and >24.1 kV), unstable jetting occurred.

The jetting behavior of the PEG/ethanol/SPIONs formulation is shown in the Supporting Information (Figure S3B and Table S1B). Unlike previous formulations, the PEG/ethanol/SPIONs medium is more inconsistent even when the flow rate is set at 15 μL/min. Numerous articles have used flow rates in this region to form polymeric particles by ES methods.<sup>34</sup> This increase in inconsistency is attributed to the presence of the SPIONs in the formulation. The SPIONs can agglomerate, which can lead to intermittent nozzle blockage and media flow, and subsequently, a greater flow rate (or a burst of increased flow) is required to maintain continuous media infusion. In general, this system (PEG/ethanol/SPIONs) is found to be unstable throughout the mapping process. For example, when continuous flow is achieved (>15 μL/min) at an applied voltage below 8 kV, only microdripping is observed, which is a precursor to the stable jetting mode. However, when the applied voltage is increased above 8 kV, unstable jetting is observed. This, again, is attributed to the effects of a nonhomogeneous medium (particle agglomeration).

The jetting behavior of the tristearin/dichloromethane formulation (Supporting Information, Figure S3C and Table S1C) was found to display inconsistent flow behavior at flow rates below 6.5 μL/min, suggesting insufficient infusion of material. By increasing the flow rate (6.6–12.5 μL/min), the dripping mode was again observed with jetting behavior. However, at flow rates of 12.5, 25, and 50 μL/min and applied voltages of 7–18.8, 11.8–19.2, and 11–15.2 kV, respectively, a stable jetting window was established. An unstable jetting mode was observed either above or below these applied voltages.

The final formulation using the coaxial electrospaying (CO-ES) process, consisting of tristearin (2 w/v %) in the outer needle and PEG/ethanol (5 w/v %), genistein (1 mg/mL), SPIONs (0.5 w/v %), and BODIPY (0.01 mg/mL) in the inner needle, is shown in Figure 2A and Table S1D (Supporting

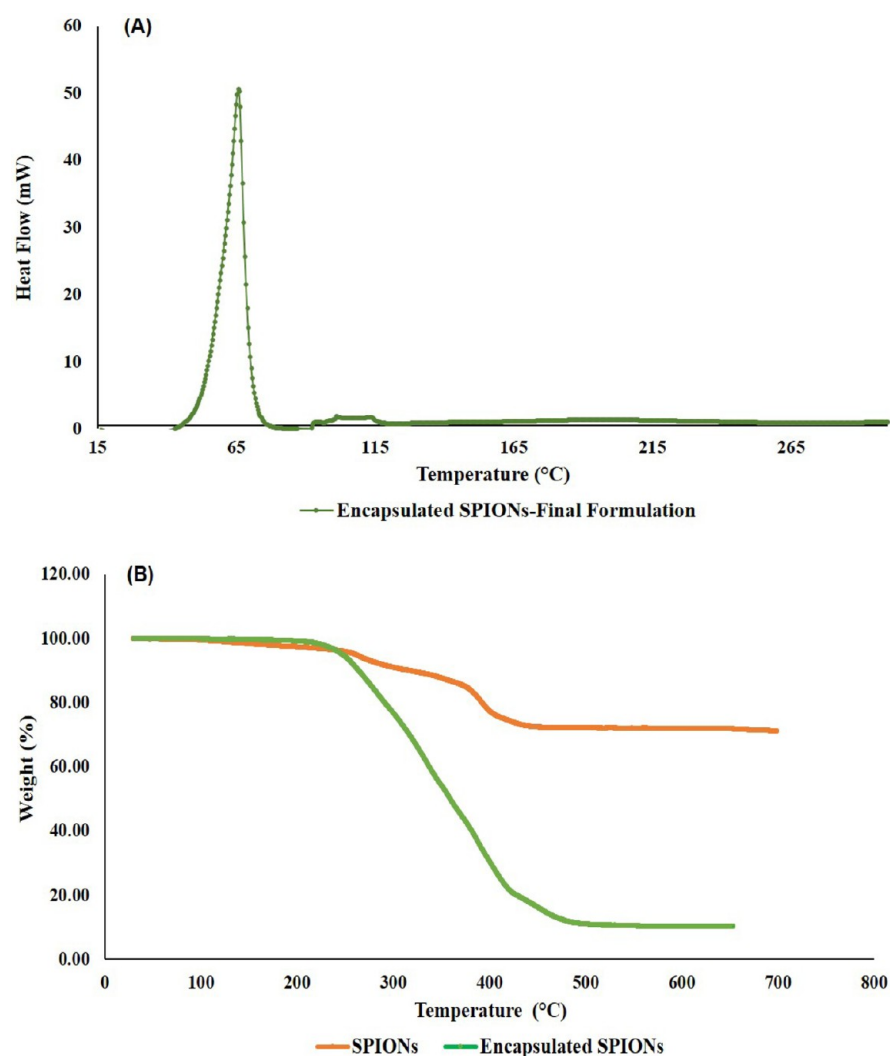


**Figure 3.** Thermogravimetric analysis of SPIONs and encapsulated SPIONs: (A) DSC and (B) related TGA.

Information). The flow rate in the inner needle was fixed at 20  $\mu\text{L}/\text{min}$ . An inconsistent combined flow was observed for flow rates up to 19  $\mu\text{L}/\text{min}$  and applied voltages in the range 1–30 kV. Dripping mode behavior of the coaxial process was observed when increasing the flow rate to  $\sim 40$   $\mu\text{L}/\text{min}$  with an applied voltage of 8 kV. However, when using the same flow rate and increasing the applied voltage to 30 kV, an unstable jetting window was observed. An operating window was thus established for stable jetting at 25, 27.5–33, and 33–35.2  $\mu\text{L}/\text{min}$  with applied voltages of 13, 15, and 12.5 kV, respectively. An uneven coflow was observed at higher flow rates (40.2–50  $\mu\text{L}/\text{min}$ ). Figure 2B–F shows the jetting modes of electro-spraying during the jetting and mode mapping process.

**Electrospray Encapsulation.** The coaxial electro-spray process is an emerging method to encapsulate biomolecules and actives. It demonstrates clear benefits over existing platforms. First, the process is operational at the ambient temperature; permitting the encapsulation of sensitive molecules and active pharmaceutical ingredients (APIs).<sup>34</sup> Second, the process is low shear and prepares several interparticle compartments in a single engineering step; unlike several chemical techniques, which require the use of numerous solvents and medium transfer phases. In this regard, the technique has shown higher encapsulation efficiencies for

biomolecules when compared to other techniques, as material loss is reduced between process steps. More recently, single nozzle techniques are being explored for scalability, which are showing promise. The process parameters are facile; providing morphological and size variation during engineering.<sup>20</sup> Finally, since device size can be varied from a small hand-held set to multiple capillaries, the underlying principle can fit into several product development settings.<sup>35</sup>

**Spectroscopic and Analytical Characterization of Electro-sprayed Particles.** Fourier transform infrared (FTIR) spectroscopy provided evidence for the presence of iron oxide within the encapsulated structure, with Fe–O absorptions at 530 and 400  $\text{cm}^{-1}$ .<sup>36,37</sup> The spectra for the encapsulated SPIONs also show the presence of C–O absorptions for the PEG component in the region from 1097 to 1341  $\text{cm}^{-1}$ , while the band at 1468  $\text{cm}^{-1}$  can be assigned to the C–H bending vibrations from the oleic acid chain.<sup>38</sup> The vibrational band at 1736  $\text{cm}^{-1}$  indicates the presence of tristearin (C=O stretch) in the encapsulated particles.<sup>39</sup> The peaks at 2849 and 2914  $\text{cm}^{-1}$  could be assigned to C–H stretches of the aliphatic chains.<sup>37</sup> In addition, direct comparison of the FTIR spectra of the individual constituents (tristearin, PEG, SPIONs, and genistein) against the encapsulated assembly confirms the presence of these components in

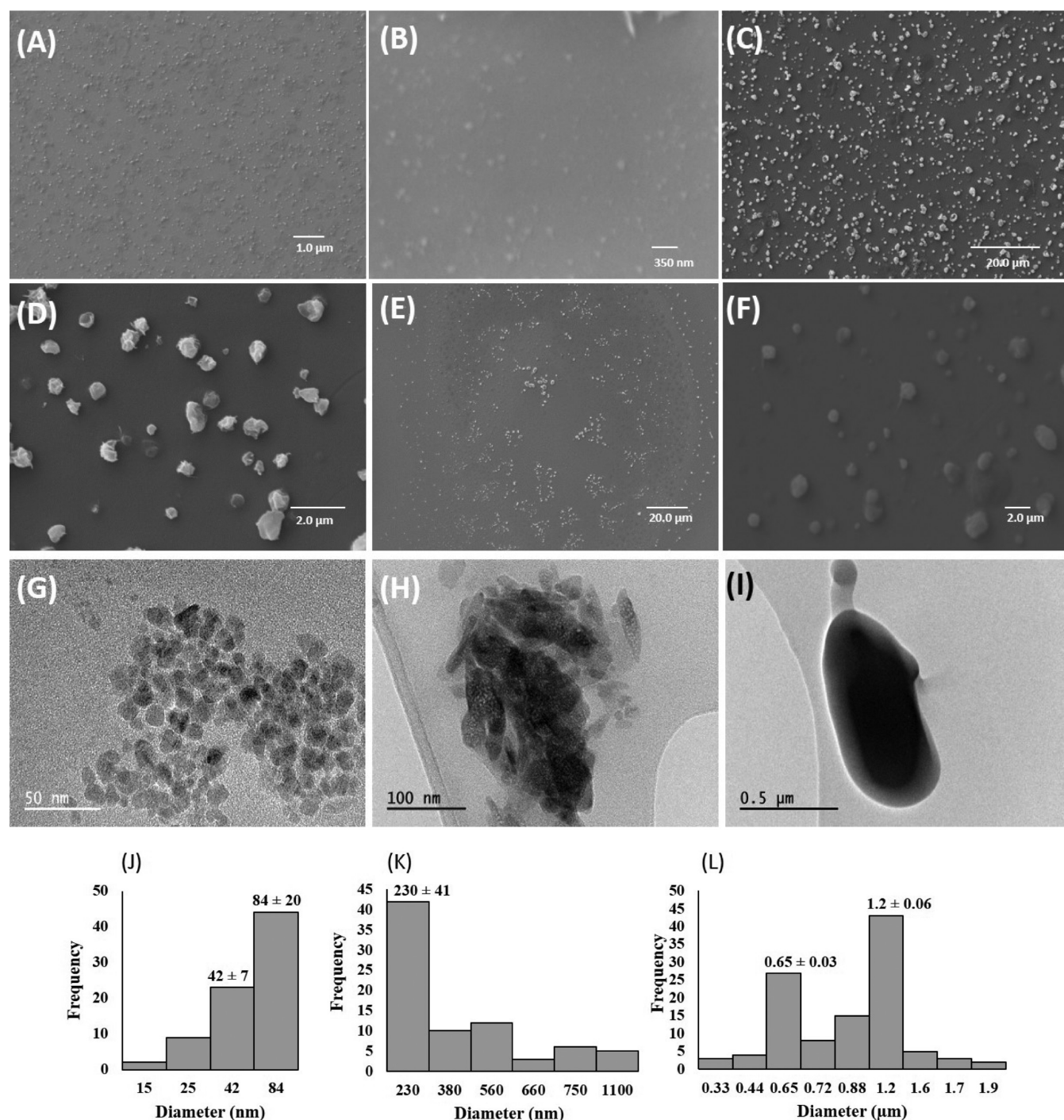


**Figure 4.** Scanning and transmission electron microscopy (SEM, TEM) images showing tristearin NPs, composite tristearin and SPIONs, and encapsulated SPIONs. (A) Electron micrograph of tristearin NPs using single-needle ES at an operating voltage of 15–18.8 kV and flow rate of 12.5  $\mu\text{L}/\text{min}$ , scale bar 1000 nm, and (B) at higher magnification, scale bar 350 nm; (C) electron micrograph of composite tristearin–SPIONs using single-needle ES at an operating voltage of 16–19 kV and flow rate of 25  $\mu\text{L}/\text{min}$ , scale bar 20000 nm, and (D) with higher magnification, scale bar 2000 nm; (E) electron micrograph of encapsulated SPIONs with tristearin (outer layer) and SPIONs, PEG, genistein, and BODIPY (inner layer) using CO-ES needles at an operating voltage of 15 kV and a flow rate of 20 and 25  $\mu\text{L}/\text{min}$  for inner and outer needles, respectively, scale bar 20000 nm, and (F) at higher magnification, scale bar 2000 nm. (G) TEM image of synthesized SPIONs, scale bar 50 nm; (H) TEM image of composite tristearin–SPIONs (single-needle ES), scale bar 100 nm; (I) TEM image showing the encapsulated SPIONs with core–shell structures, scale bar 500 nm. (J–L) Size distribution of tristearin NPs, composite tristearin-SPIONs, and encapsulated SPIONs.

the final formulation of the encapsulated SPIONs (Supporting Information, Figure S4A–E).

Figure 3 shows the differential scanning calorimetric (DSC) and thermogravimetric (TGA) analysis data for the encapsulated SPIONs and parent SPIONs. For the SPIONs alone, the

DSC curve exhibits no particular heat change or peak during scanning (Supporting Information, Figure S5A) and the corresponding TGA curve displays a weight loss of 28% between 126 to 441  $^{\circ}\text{C}$ , which is attributed to the gasification of the small molecules present (e.g., water, oleic acid).<sup>34</sup> The DSC

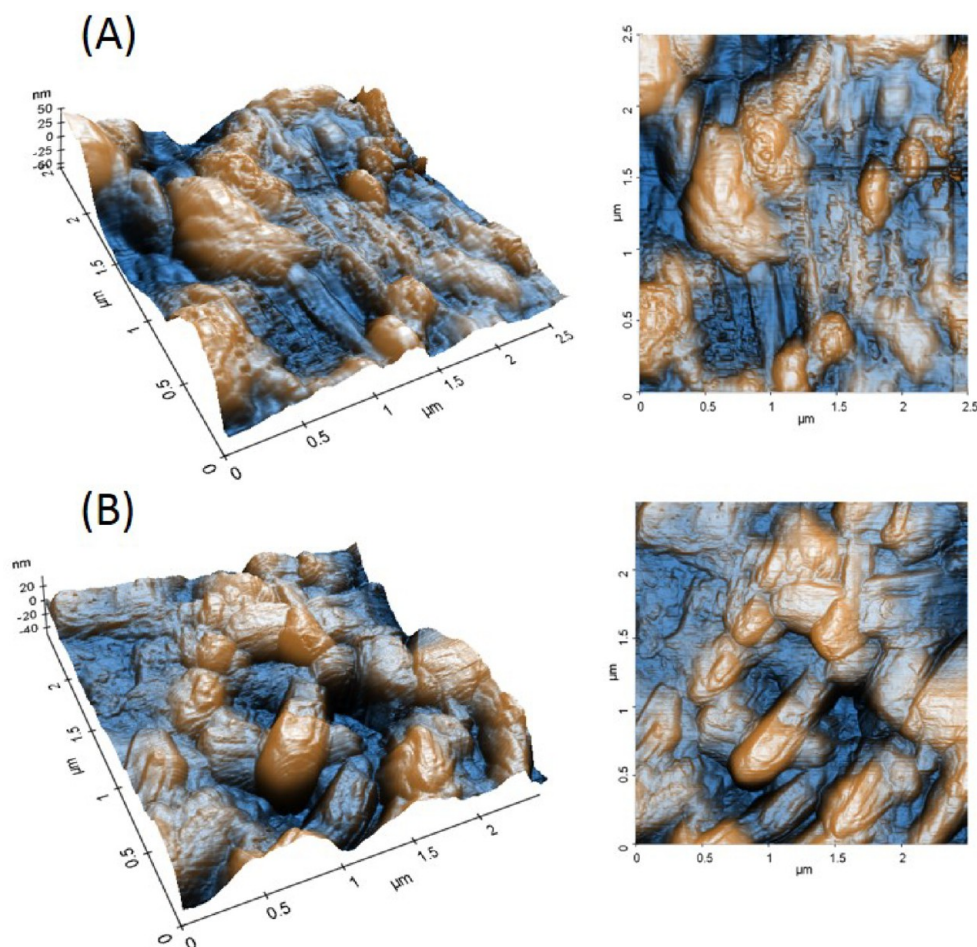


**Figure 5.** Atomic force microscopy (AFM) of composite tristearin–SPIONs (A) and the final formulation of encapsulated SPIONs (B).

curve of the tristearin and PEG indicate a crystallization event observed between 44 and 77 °C, which is attributed to their melting transitions<sup>40</sup> (Supporting Information, Figure S5B). The DSC of the encapsulated SPIONs (final formulation) reveals a crystallization peak between 47 and 76 °C but no notable heat change or crystallization observed for the final formulation. These results suggest the presence of intermolecular interaction between the materials within the encapsulated particles (Figure 3A). The TGA (Figure 3B) of the encapsulated SPIONs and parent SPIONs show gradual decomposition between 300 and 400 °C, reflecting the decomposition of the organic components in the outer layers of the SPIONs (oleic acid and solvent) encapsulated SPIONs (tristearin, PEG, genistein, and BODIPY). From the TGA it can be seen that approximately 10% wt. of the encapsulated SPIONs is inorganic iron oxide material.

**Microscopy Analysis and Zeta-Potential.** To evaluate the size and morphology of the electrosprayed particles under stable conditions, SEM and TEM were used. Electron micrographs of tristearin nanoparticles (2 w/v %) using single needle ES at an operating voltage of 15–18.8 kV and flow rate of 12.5  $\mu\text{L}/\text{min}$  show spherical particles (Figure 4A,B). The particle size and size distribution of particles was measured using Carl Zeiss, SmartTiffV3 software and the mean value of three data sets recorded. At least 50 particles were chosen randomly from the SEM image ( $84 \pm 20$  nm, Figure 4J). Figure 4C,D shows the generated composite tristearin–SPIONs [tristearin in dichloromethane (2 w/v %) and SPIONs (0.5

w/v %)] using the single needle ES process at an operating voltage of 16–19 kV and a flow rate of 25  $\mu\text{L}/\text{min}$  with an average particle size of  $230 \pm 41$  nm (Figure 4K). However, less uniform and varied particle morphology is also apparent.

For the final formulation, the CO-ES process was employed using tristearin (outer needle) and SPIONs, PEG, genistein, and BODIPY (inner needle) to generate a more uniform particle formulation, as shown in Figure 4E,F (at higher magnification). Encapsulated SPIONs were generated with a mean size distribution of approximately  $650 \pm 30$  to  $1200 \pm 60$  nm (Figure 4L). The synthesized SPIONs, with average size between 10–15 nm (Figure 4G), were used for the final encapsulation formulation. To verify the SPIONs encapsulation in the final formulation (using CO-ES) and the composite tristearin–SPIONs (single-needle ES) material, TEM was used. Figure 4H shows the SPIONs, which are dispersed throughout the composite system. In addition, greater roughness of the surface is apparent, which is attributed to a matrix mixture of SPIONs and tristearin polymer.

Sample I (Figure 4I) exhibits a well-defined core–shell structure, with SPIONs bound inside a smooth polymeric surface. The encapsulation of SPIONs within the outer layer (tristearin) is clearly visible from the change in contrast. The difference in shape is attributed to agglomerated SPIONs. In conventional electrospraying, where polymer and low molecular weight additives are used (e.g., drugs), the drying process is simple and the lowest energy conformation for particle formation is spherical. In this instance, we hypothesize that

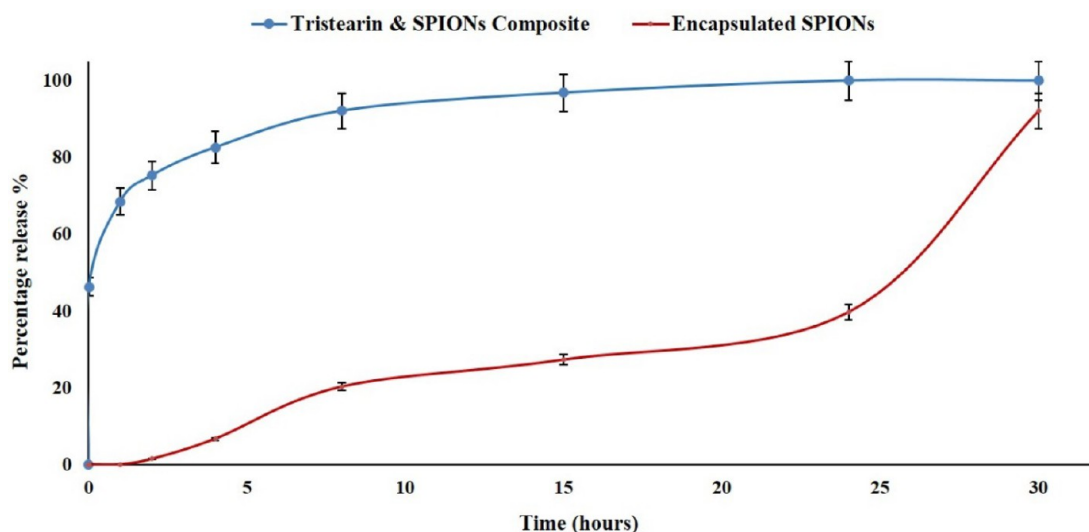


**Figure 6.** *In vitro* release profile of composite tristearin–SPIONs (blue) and the encapsulated SPIONs (red).

the small size of the particles and the presence of SPIONs agglomerates deform the particle shape during the drying process.

Atomic force microscopy (AFM) reveals important surface topography characteristics of specific particle samples. Two samples were prepared for AFM analysis; a composite sample comprising SPIONs embedded in a tristearin polymeric matrix (Figure 5A) and the final encapsulation formulation comprising SPIONs with a tristearin core–shell (Figure 5B). The size distribution for both samples correlates well with findings obtained from electron micrographs. There is also clear evidence of particle merging or coalescence upon drying for both sample types. More interestingly, the surface roughness further supports the site-specific incorporation of magnetic nanoparticles. The composite mixture possesses a greater roughness [roughness measurements (Rms)  $\approx$  90 nm] over the scanned area (Figure 5A) when compared to the encapsulated core–shell particle system (Rms  $\approx$  14 nm) (Figure 5B). This suggests particles are embedded within the core–shell for the encapsulated system and are dispersed throughout the matrix for the composite system; even on the outer surface. This further supports the possibility of localizing magnetic particles in the core–shell system along with chosen active molecules, which could reduce leaching of particles and drugs from within the encapsulated assembly.  $\zeta$ -Potential for blank tristearin and final formulation particles were  $-4.9$  and  $-22.9$  mV, respectively. Even though tristearin is used in both particulate systems (neat and encapsulating shell morphologies), a clear difference in their respective  $\zeta$ -potential values is observed. The final formulation, which hosts SPIONs, is responsible for the marked difference between the two values. Previous reports have shown iron oxide nanoparticles to possess  $\zeta$ -potential values similar to our core–shell composite system.<sup>41</sup> As the value moves away from zero, greater dispersibility is expected arising due to enhanced electrostatic repulsive forces. Furthermore, this also suggests while the core–shell system can encapsulate SPIONs, the impact of charge is still present. Encapsulation of SPIONs within variants of a modified polymeric shell have displayed different  $\zeta$ -potential values ranging from  $\sim 15.7$  to  $-0.2$  mV.<sup>42</sup> This indicates SPION encapsulation material and excipient formulation also affect the dispersibility of overall formulated particles in the test medium.

**Drug Release.** Core–shell micron and submicron particles have great potential as novel cancer therapies, both for improving the accumulation of drugs in tumor models and for minimizing their toxic side effects; for example, SPIONs encapsulated in liposomes have proven effective for the treatment of breast cancer tumors.<sup>43</sup> Genistein was selected as a model drug compound for drug release studies. It has recently demonstrated to inhibit the growth of human colon cancer cells and promoted apoptosis in a dose-dependent manner.<sup>44</sup> The effects of genistein on other various types of cancer has recently been demonstrated.<sup>45</sup>

The *in vitro* release profile of the composite tristearin–SPIONs and the final formulation of encapsulated SPIONs is shown in Figure 6. The composite tristearin–SPIONs demonstrated a burst followed by a slower second phase release profile. This can be attributed to the morphology of the composite particles, where the model drug (genistein) was dispersed throughout the particles and/or embedded on the surface. A burst release of 46% at 16 min was demonstrated. This second phase continued until the plateau point for the profile. The release of genistein at selected time points was 2 h (75%), 8 h (92%), and 15 h (96%). A further 4% release was also demonstrated at 30 h (100%).

In contrast, the encapsulated system demonstrated a triphasic release pattern. This has been demonstrated previously for other encapsulation techniques.<sup>46</sup> The first phase of a typical triphasic release profile is generally a burst release; however, in this instance, an atypical gradual release of genistein ( $\sim 20\%$ ) was observed up to 8 h. This is attributed to superficial matrix and surface adsorbed genistein being released from the multimodal particles. The second phase of the triphasic release profile displayed a plateaued gradual release of genistein of  $\sim 40\%$  up to 24 h. Partial hydrolysis and degradation of the tristearin matrix is thought to result in diffusion of genistein from the particles.<sup>47</sup> A rapid release of genistein with 92% at 30 h is observed, most likely due to the total degradation of the particle matrix. The much slower drug release profile of the encapsulated particle may be useful for a more controlled release at the target site where the administration of a drug over a longer period of time may be more beneficial. Higuchi and Korsmeyer–Peppas models were applied to the data obtained for the final particle formulation. The Higuchi model describes

drug dissolution from different types of modified polymeric release dosage forms. The Higuchi model can be represented using eq 2<sup>48</sup>

$$Mt = k_H \sqrt{t} \quad (2)$$

where  $M_t$  is the quantity of cumulative drug released at time  $t$  and  $k_H$  is the Higuchi constant. The cumulative release of Genistein from all three samples was plotted as a function of the square root of time.

Korsmeyer–Peppas model was used to investigate a diffusive-type mechanism from the polymeric matrix and is shown in eq 3

$$\frac{M_t}{M_\infty} = kt^n \quad (3)$$

where  $M_t/M_\infty$  is the proportion of genistein released at time  $t$ ,  $k$  is the release rate constant, and  $n$  is the release exponent and is the factor that determines mechanism of drug release. The release exponent is derived using eq 4

$$\log\left(\frac{M_t}{M_\infty} \times 100\right) = n \log t \times \log k \quad (4)$$

The core–shell encapsulated SPIONs displayed an  $R^2$  value of 0.7725, and the  $n$  value was 0.885 (for the Korsmeyer–Peppas Model). This indicated the mechanism was non-Fickian diffusion. In addition, the Higuchi model also indicated non-Fickian mechanisms (0.7728).<sup>49</sup>

**MTT Cytotoxicity Assay.** The cytotoxicity of particles depends on a number of factors, such as the composition of the material, the shape and size (particle morphology), and surface charge. For example, for nonphagocytic cells, increased toxicity is associated with the nanoparticle size when compared with larger, micron-sized particles.<sup>50,51</sup> This was also investigated for NPs smaller than 100 nm, and this confirmed that smaller particles are often more toxic than larger particles (quantum dots and titanium dioxide NPs).<sup>52,53</sup> Although, no differences were observed when compared with silica particles with average size between 10 and 100 nm and 45  $\mu\text{m}$ .<sup>54</sup> Okuda-Shimazaki et al. demonstrated that aggregation can also affect the cytotoxicity of NPs.<sup>55</sup> In addition, the toxicity exhibited by some particles could also be due to contamination, solubility, and adsorption of compounds. This can be significantly affected by the particle concentration, the cell type used for the cytotoxicity study, the cell density, the composition of the medium, and even the temperature.<sup>56</sup>

The MTT [3(4,5-dimethylthiazol-2-yl)-2,5-diphenyltetrazolium bromide] cell viability assay method was used to evaluate the cell viability in the presence of the NPs.<sup>57</sup> The results of MTT assay for encapsulated SPIONs and tristearin NPs confirmed cellular toxicity only at the higher concentration of encapsulated particles (1 mg/mL) when compared to the control (HeLa cells + media). This toxicity could be due to the physiological effect of the particles, or it could possibly be related to traces of the dichloromethane solvent used in their synthesis, which could theoretically reach toxic levels at higher particle concentrations. There were no significant differences observed in toxicity between the encapsulated SPIONs and tristearin NPs. The MTT assay of encapsulated SPIONs and the tristearin NPs with concentrations lower than 0.5 mg/mL showed low levels of toxicity, demonstrating cellular tolerance to the encapsulated SPIONs loaded with genistein (Bonferroni test, \* $P < 0.05$  relative to control) (Figure 7).

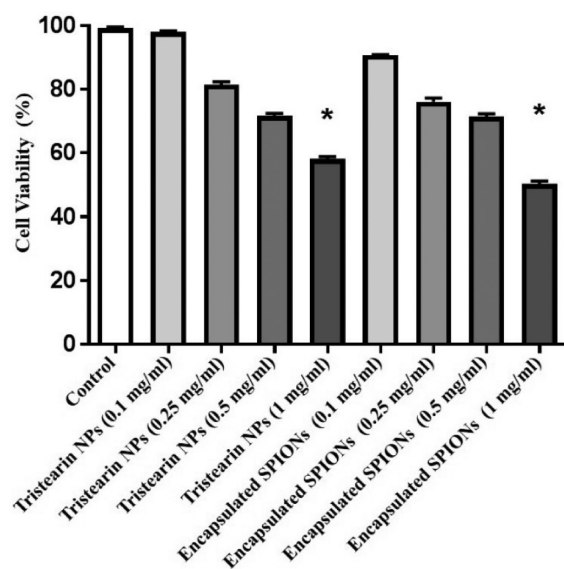


**Figure 7.** Cell viability assay data of tristearin NPs and the encapsulated SPIONs using HeLa cells (control being without NPs) after 24 h incubation of the cells (data were analyzed using one-way ANOVA with Bonferroni test, \* $p < 0.05$  relative to control).

**Relaxivity Measurements.** In order to examine the potential of the encapsulated SPIONs to act as a contrast agent for magnetic resonance imaging (MRI), transverse relaxation measurements were carried out.  $T_2$  was measured at 9.4 T (400 MHz) at ambient temperature. The transverse ( $r_2$ ) relaxivity was determined using eq 5:

$$\left(\frac{1}{T_2} - \frac{1}{T_0}\right) = r_2[\text{SPIONs}] \quad (5)$$

where  $T_0$  and  $T_2$  are the transverse relaxation times of water and of the samples with increasing SPIONs concentration.

From the slope  $\left(\frac{1}{T_2} - \frac{1}{T_0}\right)$  versus the SPION concentration, a transverse relaxivity ( $r_2$ ) value of 0.214 ( $\text{mM}^{-1} \text{s}^{-1}$ ) was obtained (Supporting Information, Figure S6). This can be compared to the transverse relaxivity ( $r_2$ ) of the coaxial electrospayed particles without SPIONs ( $0.045 \text{ mM}^{-1} \text{ s}^{-1}$ , Supporting Information, Figure S7), indicating increased  $r_2$  relaxivity. The low  $r_2$  relaxivity of the encapsulated SPIONs can be attributed to the coating layer (tristearin) preventing water molecules being within the range of the magnetic field generated by the SPIONs as well as the low SPIONs concentration into the particulate system (5 w/w % loading in 1 mg of collected particles) in the final formulation.<sup>58,59</sup>

**Confocal Imaging and Cellular Uptake.** Surface characteristics (hydrophobicity and charge) are also important in the cellular uptake of materials for medical applications. While a positive charge seems to improve the efficacy of imaging and drug delivery, higher levels of cytotoxicity have also been reported for such species.<sup>60</sup> The positive and negative charge effects on nonphagocytic cells were probed to reveal that materials with a positively charged (cationic) surface, such as polystyrene and iron oxide, have a higher cellular uptake when compared to negatively charged particles.<sup>61,62</sup> It was also reported that positively charged gold particles, SPIONs, lipid particles, chitosan, and polymeric and polystyrene particles are

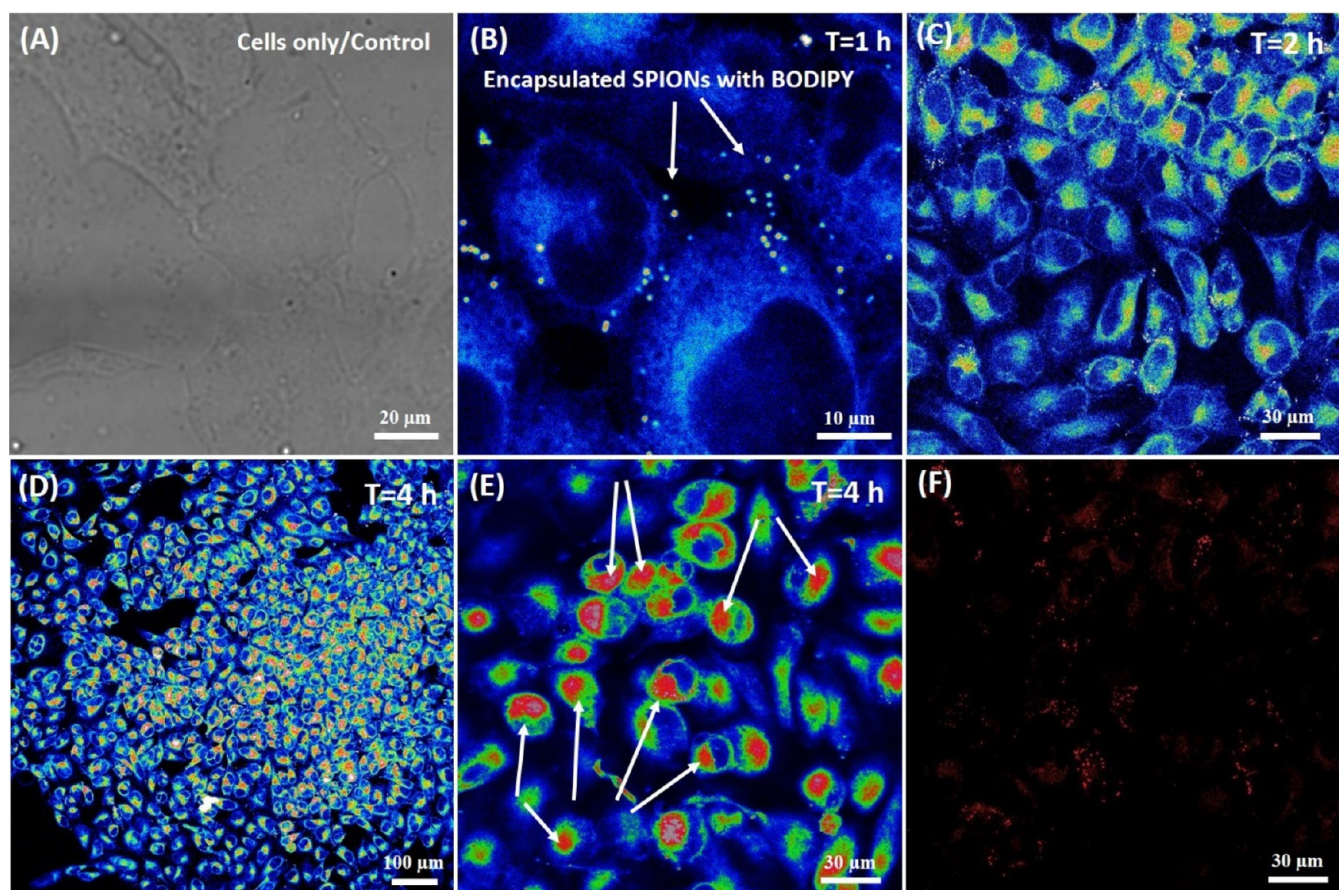


**Figure 8.** Cell uptake and accumulation of the encapsulated SPIONs into HeLa cells incubated for 1, 2, and 4 h. (A) Living HeLa cells visualized by Leica SP5 inverted confocal microscope, scale bar 20  $\mu\text{m}$ ; (B) encapsulated SPIONs with BODIPY and HeLa cells incubated for 1 h, scale bar 10  $\mu\text{m}$ ; (C) cell uptake after 2 h of incubation, scale bar 30  $\mu\text{m}$ ; (D) cell uptake after 4 h of incubation, scale bar 100  $\mu\text{m}$ ; (E) 4 h incubation with higher magnification, scale bar 30  $\mu\text{m}$ ; (F) image showing presence of BODIPY fluorescent dye after 4 h, scale bar 30  $\mu\text{m}$ .

taken up by cells to a much greater extent compared to otherwise similar anionic particles.<sup>63–67</sup>

Figure 8 shows uptake in HeLa cells of the encapsulated particles at different time points (1, 2, and 4 h). Internalization of encapsulated SPIONs was observed in HeLa cell lines with only 4 h of incubation. Figure 8A shows HeLa cells after 24 h of incubation (control) before adding the encapsulated particles. Figure 8B shows the presence of particles and the adherence of encapsulated SPIONs to the surface of the HeLa cells. Cell uptake of encapsulated SPIONs and internalization in the cells<sup>68</sup> was monitored with an image shown after 2 h (Figure 8C). Figure 8D,E (at higher magnification) demonstrates cell uptake of large encapsulated particles after 4 h of incubation. Figure 8F shows the presence of BODIPY fluorescent dye in the culture medium after 4 h. The internalization of the encapsulated SPIONs may also be related to the positively charged surface of the tristearin on the outer layer of the multimodal particle system. Earlier reports suggest that the magnetic system can be improved by modification of iron oxide NPs to render them cationic, which improves the biocompatibility and hydrophilicity significantly.<sup>69</sup>

In this study, the mean size of the final formulation of particles was in the range of 0.65–1.2  $\mu\text{m}$ , which is comparable to previous reports used for a range of *in vivo* applications.<sup>70–72</sup> The electrospray process is a multivariate process, which enables particle size scalability, based on process parameters (flow rate, applied voltage, formulation viscosity), component

geometry (e.g., nozzle), and selected formulation excipients. Furthermore, the process is operational in a single step, and the use of a filter or sieve could enable the collection of a desired particle size range. Cell internalization and external magnet localization has been shown using the current engineered particles; however, for future *in vivo* applications a reduction in particle size will be paramount.

## CONCLUSION

SPIONs with a mean diameter of 10–15 nm were successfully encapsulated into a tristearin core–shell particle system along with a model drug (genistein), a BODIPY fluorescent dye, and PEG in a single step under ambient conditions using a CO-ES process. Spectroscopic analytical methods confirmed the presence of excipients in the particle system. The encapsulated particles were much larger compared to the parent SPIONs and exhibited a mean size of  $\sim 0.65$ –1.2  $\mu\text{m}$  with evidence of a layered structure based on electron microscopy images. This increased size was the likely result of agglomeration of SPIONs during the CO-ES process. It was found that the drug release profile of genistein from the encapsulated SPIONs was much slower over a 30 h period compared to composite particles prepared via the single method and followed an atypical triphasic release. No significant toxicity was observed at 0.5 mg/mL loading for the encapsulated SPIONs based on an MTT assay. Unsurprisingly, the encapsulated SPIONs displayed limited  $r_2$  relaxivity due to the encapsulation preventing

a rapid dephasing of the nuclear spins of water molecules; however, it may be anticipated that once the shell matrix of these particles breaks down, as is observed after 30 h, then relaxivity of the “free” SPIONs would increase and therefore be more applicable for MRI imaging. Optical imaging studies of the encapsulated SPIONs show clear cellular uptake and internalization over a 4 h period. This CO-ES approach to the functionalization of SPIONs offers a straightforward and general way of coating inorganic nanoparticle materials with a polymeric drug loaded matrix. Investigations are currently underway to generate more monodisperse and smaller particles as well as diversifying the particles that can be processed in this way.

## ■ ASSOCIATED CONTENT

### Supporting Information

The Supporting Information is available free of charge on the ACS Publications website at DOI: [10.1021/acs.molpharmaceut.7b00109](https://doi.org/10.1021/acs.molpharmaceut.7b00109).

Schematic representations of SPIONs synthesis, UV–vis spectra of the synthesized SPIONs, mode mapping optimization information, FTIR of the raw materials and encapsulated SPIONs, DSC of the raw materials, and  $T_2$  relation rate data for the encapsulated tristearin NPs (without SPIONs) (PDF)

## ■ AUTHOR INFORMATION

### Corresponding Authors

\*E-mail: [philip.miller@imperial.ac.uk](mailto:philip.miller@imperial.ac.uk).

\*E-mail: [j.wilton-ely@imperial.ac.uk](mailto:j.wilton-ely@imperial.ac.uk).

\*E-mail: [m.rasekh15@imperial.ac.uk](mailto:m.rasekh15@imperial.ac.uk).

\*E-mail: [zahmad@dmu.ac.uk](mailto:zahmad@dmu.ac.uk).

### ORCID

James D. E. T. Wilton-Ely: 0000-0002-5192-3038

Philip W. Miller: 0000-0002-8394-2516

### Notes

The authors declare no competing financial interest.

## ■ ACKNOWLEDGMENTS

We are grateful to Imperial College London and the Medical Research Council (MRC grant no. MR/J015881/1) for funding. Z.A. acknowledges support from The Royal Society to develop a modified in-house built electro-spraying system. We would like to thank Khairil Jantan and Nicolas Chabloz for assistance in SPION synthesis and Jonathan Robson for providing the sample of BODIPY. Confocal microscopy was performed at the facility for imaging by light microscopy (FILM) at Imperial College London.

## ■ REFERENCES

- (1) Allen, T. M.; Cullis, P. R. Liposomal Drug Delivery Systems: From Concept to Clinical Applications. *Adv. Drug Delivery Rev.* **2013**, *65* (1), 36–48.
- (2) Lee, D.-E.; Koo, H.; Sun, I.-C.; Ryu, J. H.; Kim, K.; Kwon, I. C. Multifunctional Nanoparticles for Multimodal Imaging and Theragnosis. *Chem. Soc. Rev.* **2012**, *41* (7), 2656–2672.
- (3) Zhang, L.; Gu, F. X.; Chan, J. M.; Wang, A. Z.; Langer, R. S.; Farokhzad, O. C. Nanoparticles in Medicine: Therapeutic Applications and Developments. *Clin. Pharmacol. Ther.* **2008**, *83* (5), 761–769.
- (4) Boisselier, E.; Astruc, D. Gold Nanoparticles in Nanomedicine: Preparations, Imaging, Diagnostics, Therapies and Toxicity. *Chem. Soc. Rev.* **2009**, *38* (6), 1759–1782.
- (5) Gao, J.; Gu, H.; Xu, B. Multifunctional Magnetic Nanoparticles: Design, Synthesis, and Biomedical Applications. *Acc. Chem. Res.* **2009**, *42* (8), 1097–1107.
- (6) Thorek, D. L. J.; Chen, A. K.; Czupryna, J.; Tsourkas, A. *Ann. Biomed. Eng.* **2006**, *34* (1), 23–38.
- (7) Reddy, L. H.; Arias, J. L.; Nicolas, J.; Couvreur, P. Magnetic Nanoparticles: Design and Characterization, Toxicity and Biocompatibility, Pharmaceutical and Biomedical Applications. *Chem. Rev.* **2012**, *112*, 5818–5878.
- (8) Veisoh, O.; Gunn, J. W.; Zhang, M. Design and Fabrication of Magnetic Nanoparticles for Targeted Drug Delivery and Imaging. *Adv. Drug Delivery Rev.* **2010**, *62* (3), 284–304.
- (9) Xie, J.; Lee, S.; Chen, X. Nanoparticle-Based Theranostic Agents. *Adv. Drug Delivery Rev.* **2010**, *62* (11), 1064–1079.
- (10) Peng, N.; Wu, B.; Wang, L.; He, W.; Ai, Z.; Zhang, X.; Wang, Y.; Fan, L.; Ye, Q. High Drug Loading and pH-Responsive Targeted Nanocarriers from Alginate-Modified SPIONs for Anti-Tumor Chemotherapy. *Biomater. Sci.* **2016**, *4* (12), 1802–1813.
- (11) Yu, M. K.; Jeong, Y. Y.; Park, J.; Park, S.; Kim, J. W.; Min, J. J.; Kim, K.; Jon, S. Drug-Loaded Superparamagnetic Iron Oxide Nanoparticles for Combined Cancer Imaging and Therapy in Vivo. *Angew. Chem., Int. Ed.* **2008**, *47* (29), 5362–5365.
- (12) Maeng, J. H.; Lee, D.-H.; Jung, K. H.; Bae, Y.-H.; Park, I.-S.; Jeong, S.; Jeon, Y.-S.; Shim, C.-K.; Kim, W.; Kim, J.; Lee, J.; Lee, Y.-M.; Kim, J.-H.; Kim, W.-H.; Hong, S.-S. Multifunctional Doxorubicin Loaded Superparamagnetic Iron Oxide Nanoparticles for Chemotherapy and Magnetic Resonance Imaging in Liver Cancer. *Biomaterials* **2010**, *31* (18), 4995–5006.
- (13) Kievit, F. M.; Wang, F. Y.; Fang, C.; Mok, H.; Wang, K.; Silber, J. R.; Ellenbogen, R. G.; Zhang, M. Doxorubicin Loaded Iron Oxide Nanoparticles Overcome Multidrug Resistance in Cancer in Vitro. *J. Controlled Release* **2011**, *152* (1), 76–83.
- (14) Akbarzadeh, A.; Samiei, M.; Joo, S. W.; Anzaby, M.; Hanifehpour, Y.; Nasrabadi, H. T.; Davaran, S. Synthesis, Characterization and in Vitro Studies of Doxorubicin-Loaded Magnetic Nanoparticles Grafted to Smart Copolymers on A549 Lung Cancer Cell Line. *J. Nanobiotechnol.* **2012**, *10* (1), 46.
- (15) Ferrari, M. Cancer Nanotechnology: Opportunities and Challenges. *Nat. Rev. Cancer* **2005**, *5* (3), 161–171.
- (16) Mehnert, W.; Mäder, K. Solid Lipid Nanoparticles: Production, Characterization and Applications. *Adv. Drug Delivery Rev.* **2001**, *47* (2–3), 165–196.
- (17) Bunjes, H.; Drechsler, M.; Koch, M. H. J.; Westesen, K. Incorporation of the Model Drug Ubidecarenone into Solid Lipid Nanoparticles. *Pharm. Res.* **2001**, *18* (3), 287–293.
- (18) Müller, R. H.; Mäder, K.; Gohla, S. Solid Lipid Nanoparticles (SLN) for Controlled Drug Delivery – a Review of the State of the Art. *Eur. J. Pharm. Biopharm.* **2000**, *50* (1), 161–177.
- (19) Chen, R.; Wang, S.; Zhang, J.; Chen, M.; Wang, Y. Aloe-Emodin Loaded Solid Lipid Nanoparticles: Formulation Design and in Vitro Anti-Cancer Study. *Drug Delivery* **2015**, *22* (5), 666–674.
- (20) Mehta, P.; Haj-Ahmad, R.; Rasekh, M.; Arshad, M. S.; Smith, A.; van der Merwe, S. M.; Li, X.; Chang, M.-W.; Ahmad, Z. Pharmaceutical and Biomaterial Engineering via Electrohydrodynamic Atomization Technologies. *Drug Discovery Today* **2017**, *22* (1), 157–165.
- (21) Rasekh, M.; Smith, A.; Arshad, M. S.; Gunduz, O.; Van der Merwe, S. M.; Smith, G.; Ahmad, Z. Electrohydrodynamic Preparation of Nanomedicines. *Curr. Top. Med. Chem.* **2015**, *15* (22), 2316–2327.
- (22) Rasekh, M.; Karavasili, C.; Soong, Y. L.; Bouropoulos, N.; Morris, M.; Armitage, D.; Li, X.; Fatouros, D. G.; Ahmad, Z. Electrospun PVP–indomethacin Constituents for Transdermal Dressings and Drug Delivery Devices. *Int. J. Pharm.* **2014**, *473* (1–2), 95–104.
- (23) Rasekh, M.; Ahmad, Z.; Frangos, C. C.; Bozec, L.; Edirisinghe, M.; Day, R. M. Spatial and Temporal Evaluation of Cell Attachment to Printed Polycaprolactone Microfibres. *Acta Biomater.* **2013**, *9* (2), 5052–5062.

- (24) Kang, Y. S.; Risbud, S.; Rabolt, J. F.; Stroeve, P. Synthesis and Characterization of Nanometer-Size Fe<sub>3</sub>O<sub>4</sub> and  $\gamma$ -Fe<sub>2</sub>O<sub>3</sub> Particles. *Chem. Mater.* **1996**, *8* (9), 2209–2211.
- (25) Yin, Z.; Tam, A. Y.; Wong, K. M.; Tao, C. H.; Li, B.; Poon, C. T.; Wu, L.; Yam, V. W. Functionalized BODIPY with Various Sensory Units—a Versatile Colorimetric and Luminescent Probe for pH and Ions. *Dalton Trans.* **2012**, *41* (37), 11340–11350.
- (26) Feng, J.; Mao, J.; Wen, X.; Tu, M. Ultrasonic-Assisted in Situ Synthesis and Characterization of Superparamagnetic Fe<sub>3</sub>O<sub>4</sub> Nanoparticles. *J. Alloys Compd.* **2011**, *509* (37), 9093–9097.
- (27) Rahbari, R.; Sheahan, T.; Modes, V.; Collier, P.; Macfarlane, C.; Badge, R. M. A Novel L1 Retrotransposon Marker for HeLa Cell Line Identification. *Biotechniques* **2009**, *46* (4), 277–284.
- (28) Smolensky, E. D.; Neary, M. C.; Zhou, Y.; Berquo, T. S.; Pierre, V. C. Fe<sub>3</sub>O<sub>4</sub>@organic@Au: Core-Shell Nanocomposites with High Saturation Magnetisation as Magnetoplasmonic MRI Contrast Agents. *Chem. Commun.* **2011**, *47* (7), 2149–2151.
- (29) Polkowski, K.; Mazurek, A. P. Biological Properties of Genistein. A Review of in Vitro and in Vivo Data. *Acta Pol. Pharm.* **2000**, *57*, 135–155.
- (30) Lobovkina, T.; Jacobson, G. B.; Gonzalez-Gonzalez, E.; Hickerson, R. P.; Leake, D.; Kaspar, R. L.; Contag, C. H.; Zare, R. N. In Vivo Sustained Release of siRNA from Solid Lipid Nanoparticles. *ACS Nano* **2011**, *5* (12), 9977–9983.
- (31) Hashem, F. M.; Nasr, M.; Fathy, G.; Ismail, A. Formulation and In Vitro and In Vivo Evaluation of Lipid-Based Terbutaline Sulphate Bi-Layer Tablets for Once-Daily Administration. *AAPS PharmSciTech* **2016**, *17* (3), 727–734.
- (32) Ahmad, Z.; Rasekh, M.; Edirisinghe, M. Electrohydrodynamic Direct Writing of Biomedical Polymers and Composites. *Macromol. Mater. Eng.* **2010**, *295* (4), 315–319.
- (33) Rasekh, M.; Young, C.; Roldo, M.; Lancien, F.; Le Mevel, J. C.; Hafizi, S.; Ahmad, Z.; Barbu, E.; Gorecki, D. Hollow-Layered Nanoparticles for Therapeutic Delivery of Peptide Prepared Using Electrospinning. *J. Mater. Sci.: Mater. Med.* **2015**, *26* (11), 256.
- (34) Xie, J.; Jiang, J.; Davoodi, P.; Srinivasan, M. P.; Wang, C.-H. Electrohydrodynamic Atomization: A Two-Decade Effort to Produce and Process Micro-/nanoparticulate Materials. *Chem. Eng. Sci.* **2015**, *125*, 32–57.
- (35) Olvera-Trejo, D.; Velásquez-García, L. F. Additively Manufactured MEMS Multiplexed Coaxial Electro Spray Sources for High-Throughput, Uniform Generation of Core-shell Microparticles. *Lab Chip* **2016**, *16*, 4121–4132.
- (36) Safaei-Ghomi, J.; Eshteghal, F.; Shahbazi-Alavi, H. A Facile One-Pot Ultrasound Assisted for an Efficient Synthesis of Benzo[g]-chromenes Using Fe<sub>3</sub>O<sub>4</sub>/polyethylene Glycol (PEG) Core/shell Nanoparticles. *Ultrason. Sonochem.* **2016**, *33*, 99–105.
- (37) Yan, K.; Li, H.; Wang, X.; Yi, C.; Zhang, Q.; Xu, Z.; Xu, H.; Whittaker, A. K. Self-Assembled Magnetic Luminescent Hybrid Micelles Containing Rare Earth Eu for Dual-Modality MR and Optical Imaging. *J. Mater. Chem. B* **2014**, *2* (5), 546–555.
- (38) Larsen, E. K.; Nielsen, T.; Wittenborn, T.; Rydtoft, L. M.; Lokanathan, A. R.; Hansen, L.; Ostergaard, L.; Kingshott, P.; Howard, K. A.; Besenbacher, F.; Nielsen, N. C.; Kjems, J. Accumulation of Magnetic Iron Oxide Nanoparticles Coated with Variably Sized Polyethylene Glycol in Murine Tumors. *Nanoscale* **2012**, *4* (7), 2352–2361.
- (39) Zimmermann, B.; Tkáčec, Z.; Mešić, A.; Kohler, A. Characterizing Aeroallergens by Infrared Spectroscopy of Fungal Spores and Pollen. *PLoS One* **2015**, *10* (4), e0124240.
- (40) MacNaughtan, W.; Farhat, I. A.; Himawan, C.; Starov, V. M.; Stapley, A. G. F. A Differential Scanning Calorimetry Study of the Crystallization Kinetics of Tristearin-Tripalmitin Mixtures. *J. Am. Oil Chem. Soc.* **2006**, *83* (1), 1–9.
- (41) Paik, S.-Y.-R.; Kim, J.-S.; Shin, S.; Ko, S. Characterization, Quantification, and Determination of the Toxicity of Iron Oxide Nanoparticles to the Bone Marrow Cells. *Int. J. Mol. Sci.* **2015**, *16* (9), 22243–22257.
- (42) Hayashi, K.; Nakamura, M.; Sakamoto, W.; Yogo, T.; Miki, H.; Ozaki, S.; Abe, M.; Matsumoto, T.; Ishimura, K. Superparamagnetic Nanoparticle Clusters for Cancer Theranostics Combining Magnetic Resonance Imaging and Hyperthermia Treatment. *Theranostics* **2013**, *3* (6), 366–376.
- (43) Plassat, V.; Wilhelm, C.; Marsaud, V.; Ménager, C.; Gazeau, F.; Renoir, J.-M.; Lesieur, S. Anti-Estrogen-Loaded Superparamagnetic Liposomes for Intracellular Magnetic Targeting and Treatment of Breast Cancer Tumors. *Adv. Funct. Mater.* **2011**, *21* (1), 83–92.
- (44) Zhang, Z.; Wang, C. Z.; Du, G. J.; Qi, L. W.; Calway, T.; He, T. C.; Du, W.; Yuan, C. S. Genistein Induces G2/M Cell Cycle Arrest and Apoptosis via ATM/p53-Dependent Pathway in Human Colon Cancer Cells. *Int. J. Oncol.* **2013**, *43* (1), 289–296.
- (45) Russo, M.; Russo, G. L.; Daglia, M.; Kasi, P. D.; Ravi, S.; Nabavi, S. F.; Nabavi, S. M. Understanding Genistein in Cancer: The “good” and the “bad” Effects: A Review. *Food Chem.* **2016**, *196*, 589–600.
- (46) Raiche, A. T.; Puleo, D. A. Triphasic Release Model for Multilayered Gelatin Coatings That Can Recreate Growth Factor Profiles during Wound Healing. *J. Drug Target* **2001**, *9* (6), 449–460.
- (47) Al-Rawi, M.; Diabate, S.; Weiss, C. Uptake and Intracellular Localization of Submicron and Nano-Sized SiO<sub>2</sub> Particles in HeLa Cells. *Arch. Toxicol.* **2011**, *85* (7), 813–826.
- (48) Korsmeyer, R. W.; Gurny, R.; Doelker, E.; Buri, P.; Peppas, N. A. Mechanisms of Solute Release from Porous Hydrophilic Polymers. *Int. J. Pharm.* **1983**, *15* (1), 25–35.
- (49) Siepmann, J.; Peppas, N. A. Higuchi Equation: Derivation, Applications, Use and Misuse. *Int. J. Pharm.* **2011**, *418* (1), 6–12.
- (50) Fröhlich, E.; Kuznetsov, T.; Samberger, C.; Roblegg, E.; Wrighton, C.; Pieber, T. R. Size-Dependent Effects of Nanoparticles on the Activity of Cytochrome P450 Isoenzymes. *Toxicol. Appl. Pharmacol.* **2010**, *242* (3), 326–332.
- (51) He, Q.; Zhang, Z.; Gao, Y.; Shi, J.; Li, Y. Intracellular Localization and Cytotoxicity of Spherical Mesoporous Silica Nano- and Microparticles. *Small* **2009**, *5* (23), 2722–2729.
- (52) Lovric, J.; Bazzi, H. S.; Cuie, Y.; Fortin, G. R.; Winnik, F. M.; Maysinger, D. Differences in Subcellular Distribution and Toxicity of Green and Red Emitting CdTe Quantum Dots. *J. Mol. Med.* **2005**, *83* (5), 377–385.
- (53) Zhang, Y.; Yu, W.; Jiang, X.; Lv, K.; Sun, S.; Zhang, F. Analysis of the Cytotoxicity of Differentially Sized Titanium Dioxide Nanoparticles in Murine MC3T3-E1 Preosteoblasts. *J. Mater. Sci.: Mater. Med.* **2011**, *22* (8), 1933–1945.
- (54) Cha, K. E.; Myung, H. Cytotoxic Effects of Nanoparticles Assessed in Vitro and in Vivo. *J. Microbiol. Biotechnol.* **2007**, *17* (9), 1573–1578.
- (55) Okuda-Shimazaki, J.; Takaku, S.; Kanehira, K.; Sonezaki, S.; Taniguchi, A. Effects of Titanium Dioxide Nanoparticle Aggregate Size on Gene Expression. *Int. J. Mol. Sci.* **2010**, *11* (6), 2383–2392.
- (56) Fröhlich, E. The Role of Surface Charge in Cellular Uptake and Cytotoxicity of Medical Nanoparticles. *Int. J. Nanomed.* **2012**, *7*, 5577–5591.
- (57) Mosmann, T. Rapid Colorimetric Assay for Cellular Growth and Survival: Application to Proliferation and Cytotoxicity Assays. *J. Immunol. Methods* **1983**, *65* (1–2), 55–63.
- (58) Lee, H.; Shin, T.-H.; Cheon, J.; Weissleder, R. Recent Developments in Magnetic Diagnostic Systems. *Chem. Rev.* **2015**, *115* (19), 10690–10724.
- (59) Lee, N.; Yoo, D.; Ling, D.; Cho, M. H.; Hyeon, T.; Cheon, J. Iron Oxide Based Nanoparticles for Multimodal Imaging and Magneto-responsive Therapy. *Chem. Rev.* **2015**, *115* (19), 10637–10689.
- (60) Agashe, H. B.; Dutta, T.; Garg, M.; Jain, N. K. Investigations on the Toxicological Profile of Functionalized Fifth-Generation Poly (Propylene Imine) Dendrimer. *J. Pharm. Pharmacol.* **2006**, *58* (11), 1491–1498.
- (61) Jiang, X.; Musyanovych, A.; Rocker, C.; Landfester, K.; Mailander, V.; Nienhaus, G. U. Specific Effects of Surface Carboxyl Groups on Anionic Polystyrene Particles in Their Interactions with Mesenchymal Stem Cells. *Nanoscale* **2011**, *3* (5), 2028–2035.

(62) Thorek, D. L.; Tsourkas, A. Size, Charge and Concentration Dependent Uptake of Iron Oxide Particles by Non-Phagocytic Cells. *Biomaterials* **2008**, *29* (26), 3583–3590.

(63) Brandenberger, C.; Rothen-Rutishauser, B.; Muhlfeld, C.; Schmid, O.; Ferron, G. A.; Maier, K. L.; Gehr, P.; Lenz, A. G. Effects and Uptake of Gold Nanoparticles Deposited at the Air-Liquid Interface of a Human Epithelial Airway Model. *Toxicol. Appl. Pharmacol.* **2010**, *242* (1), 56–65.

(64) Ge, Y.; Zhang, Y.; Xia, J.; Ma, M.; He, S.; Nie, F.; Gu, N. Effect of Surface Charge and Agglomerate Degree of Magnetic Iron Oxide Nanoparticles on KB Cellular Uptake in Vitro. *Colloids Surf., B* **2009**, *73* (2), 294–301.

(65) Yue, Z. G.; Wei, W.; Lv, P. P.; Yue, H.; Wang, L. Y.; Su, Z. G.; Ma, G. H. Surface Charge Affects Cellular Uptake and Intracellular Trafficking of Chitosan-Based Nanoparticles. *Biomacromolecules* **2011**, *12* (7), 2440–2446.

(66) Lunov, O.; Syrovets, T.; Loos, C.; Beil, J.; Delacher, M.; Tron, K.; Nienhaus, G. U.; Musyanovych, A.; Mailänder, V.; Landfester, K.; Simmet, T. Differential Uptake of Functionalized Polystyrene Nanoparticles by Human Macrophages and a Monocytic Cell Line. *ACS Nano* **2011**, *5* (3), 1657–1669.

(67) Mailänder, V.; Landfester, K. Interaction of Nanoparticles with Cells. *Biomacromolecules* **2009**, *10* (9), 2379–2400.

(68) Hafeli, U. O.; Riffle, J. S.; Harris-Shekhawat, L.; Carmichael-Baranauskas, A.; Mark, F.; Dailey, J. P.; Bardenstein, D. Cell Uptake and in Vitro Toxicity of Magnetic Nanoparticles Suitable for Drug Delivery. *Mol. Pharmaceutics* **2009**, *6* (5), 1417–1428.

(69) Das, M.; Dhak, P.; Gupta, S.; Mishra, D.; Maiti, T. K.; Basak, A.; Pramanik, P. Highly Biocompatible and Water-Dispersible, Amine Functionalized Magnetite Nanoparticles, Prepared by a Low Temperature, Air-Assisted Polyol Process: A New Platform for Bio-Separation and Diagnostics. *Nanotechnology* **2010**, *21* (12), 125103.

(70) Bachelder, E. M.; Pino, E. N.; Ainslie, K. M. Acetalated Dextran: A Tunable and Acid-Labile Biopolymer with Facile Synthesis and a Range of Applications. *Chem. Rev.* **2017**, *117*, 1915.

(71) Ma, S.; Tian, X. Y.; Zhang, Y.; Mu, C.; Shen, H.; Bismuth, J.; Pownall, H. J.; Huang, Y.; Wong, W. T. E-Selectin-Targeting Delivery of microRNAs by Microparticles Ameliorates Endothelial Inflammation and Atherosclerosis. *Sci. Rep.* **2016**, *6*, 22910.

(72) Garcia-Contreras, L.; Padilla-Carlin, D. J.; Sung, J.; VerBerkmoes, J.; Muttill, P.; Elbert, K.; Peloquin, C.; Edwards, D.; Hickey, A. Pharmacokinetics of Ethionamide Delivered in Spray-Dried Microparticles to the Lungs of Guinea Pigs. *J. Pharm. Sci.* **2017**, *106* (1), 331–337.